ELSEVIER

Polymer 43 (2002) 6683–6693

polymer

www.elsevier.com/locate/polymer

Fracture surface of plastic materials: the roughness exponent

Carlos Guerrero*, Edgar Reyes, Virgilio González

FIME, Pedro de Alba s/n, Cd. Universitaria, Universidad Autónoma de Nuevo León, San Nicolás de los Garza, N.L. 66450, Mexico

Received 17 June 2002; received in revised form 10 September 2002; accepted 12 September 2002

Abstract

In order to provide more evidence concerning the controversial topic, conjectured for the first time in the early 90's, that the roughness exponent of the self-affine fracture surfaces has a value close to 0.8, the self-affine behavior of fracture surfaces of both, semi-crystalline polypropylene (PP) and amorphous polystyrene (PS) was analyzed. The topography of polymeric fracture surfaces was obtained using atomic force microscopy, AFM, and the corresponding height profiles were processed using the variable bandwidth method (standard deviation criteria) to obtain the roughness exponent of the surfaces. Prior to that, the appropriate AFM operating conditions, in contact mode, were found. The average roughness exponent was 0.770 ± 0.09 for the fracture surfaces of polypropylene and 0.707 ± 0.07 for polystyrene. These results agree with values for different materials often reported in the literature that support 0.8 has a possible 'universal' value. Hence, it is considered that our results are in good agreement with the conjectured value even for polymeric materials.

Keywords: Roughness exponent; Self-affinity; Fracture surface

1. Introduction

A large number of important technological application of plastics are affected by surface properties, i.e. wetting, adhesion, printing, waterproofing, permeability, friction, and wear. Surfaces are in contact with the surroundings and the interactions between them are by far responsible for materials behavior. The information contained in the surface could be related among others, to microstructure and mechanical behavior of materials. Unfortunately, the theoretical description of surface interactions and its qualitative analysis, including interfaces, have only begun late in the past century [1,2]. In the case of fracture surfaces in particular, fractography is widely used to identify the origin of a crack or to determine what type of loading caused the crack to initiate and also to establish the direction of crack propagation. The fractographer uses a combination of experience and reference fractographs to identify specific fracture surface features. When fractures do not fit a recognized pattern, the process may be extremely difficult and highly subjective.

Fracture surfaces are typically a collection of repeated patterns, that is dimples, cleavage facets, fatigue striations or intergranular facets. Quantitative fractography has dealt with the translation of fracture features into parametric form. A prominent technique for the study of fracture surfaces is based on fracture profile generation [3]. The most common parameters for characterizing the profile quantitatively are the fractal dimension [4–6] and the roughness exponent [7–9]. With the development of the scanning probe microscopy, specifically the atomic force microscopy, AFM, the analysis of surfaces of non-conducting materials was improved. In fact, this technique allows the high resolution profiling of surfaces, recording the height of the surface topography on scales from hundreds of microns to nanometers [10,11].

Typically, the roughness of a surface with N observed heights, Z_i, is defined using the average roughness, R_{av}, Eq. (1)

$$R_{av} = \sum_{i=1}^{N} \frac{|Z_i - \bar{Z}|}{N} \tag{1}$$

or the root-mean-square roughness, R_{rms}, Eq. (2)

$$R_{rms} = \sqrt{\frac{\sum_{i=1}^{N} (Z_i - \bar{Z})^2}{N-1}} \tag{2}$$

* Corresponding author. Fax: +52-8332-0904.
E-mail address: cguerrer@ccr.dsi.uanl.mx (C. Guerrero).

0032-3861/02/$ - see front matter
PII: S0032-3861(02)00674-2

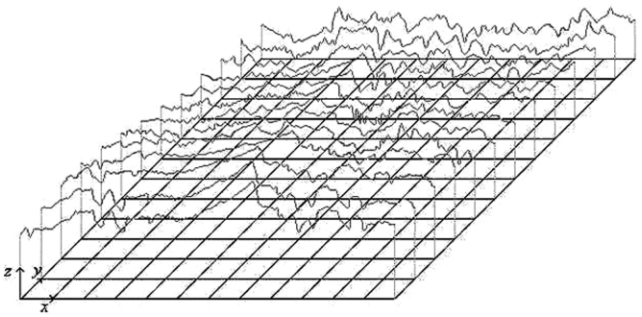

Fig. 1. Typical height profiles generated by the atomic force microscope.

Unfortunately, these two parameters are scale dependent and consequently, their magnitude would be very different for the same surface, whether the measurement is done with a profilometer (scale from mm to cm) or with an atomic force microscope (scale from Å to μm). Instead, fractal geometry allows the characterization of surface topography with scale independent parameters, such as the self-affine or roughness exponent, ζ. Fractal objects have the important invariance property under scale transformations called self-similarity. It consists of the repetition of essentially the same features as the object is viewed under increasing magnifications. The observance of this property is a sufficient condition to guarantee the existence of a fractal

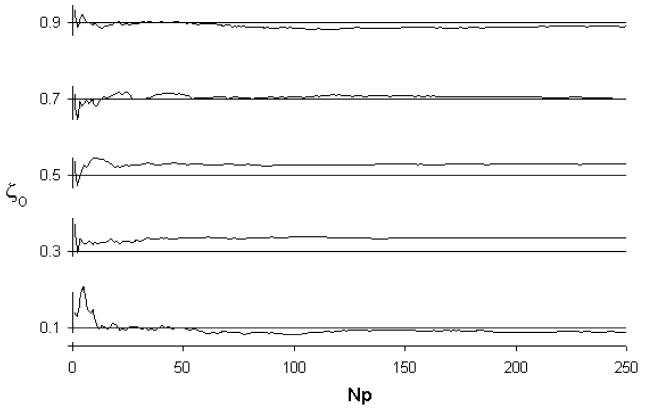

Fig. 2. Variation of the calculated roughness exponent with the number of synthetic profiles, N_p, involved on the calculus.

dimension. It should be noted that natural fractals, i.e. cauliflower, clouds, cracks, exhibit only statistical self-similarity. Unlike self-similar objects, self-affine systems, being intrinsically anisotropic, are statistical invariant only through an affine transformation, Eq. (3)

$$X \rightarrow \lambda_x X; \qquad Y \rightarrow \lambda_y Y; \qquad Z \rightarrow \lambda_z Z \qquad \text{with} \qquad \lambda_x = \lambda_y; \qquad \lambda_z = \lambda_x^{\zeta} \tag{3}$$

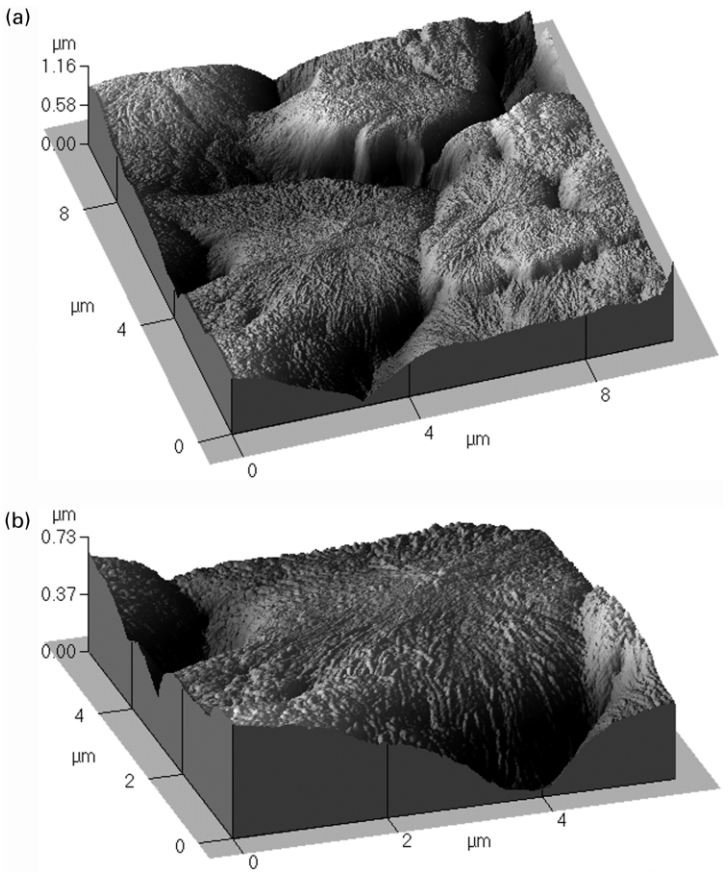

Fig. 3. 3D images of the PP film surface obtained with a contact force of 0.8 nN and a scanning frequency of 1 Hz. The scan size was: (a) $10 \times 10\ \mu m^2$, and (b) $5 \times 5\ \mu m^2$.

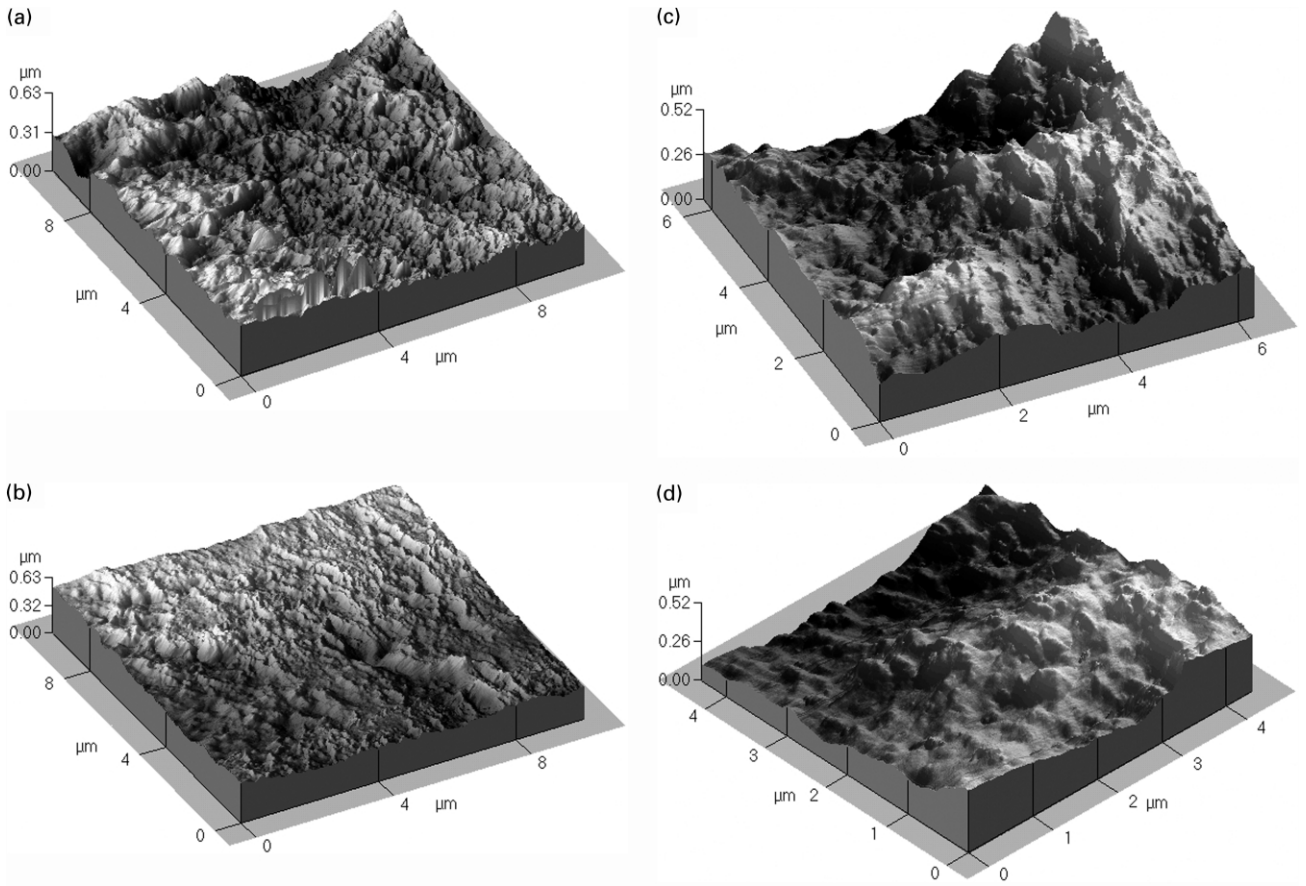

Fig. 4. 3D images of the PS film surface obtained with a contact force of 1.5 nN and a scanning frequency of 1 Hz. (a) and (b) are images of different zones of the sample; for (c) and (d) the scan size was 7×7 μm^2, and 5×5 μm^2, respectively.

ζ is the so-called roughness or self-affine exponent [12]. If Z is the height and X and Y are the coordinates within the plane perpendicular to the Z direction, ζ will take values between 0 and 1. Rougher surfaces correspond to smaller ζ values. A self-affine surface is indeed fractal up to distances of the order of a characteristic length called the correlation length, beyond which, the object is considered flat.

The roughness exponent can be evaluated knowing that, for a self-affine surface, the typical height $h(r)$ at point $r = (x^2 + y^2)^{1/2}$ satisfies the following power law equation

$$h(r) = \langle [z(r_0 + r) - z(r_0)]^2 \rangle_{r_0}^{1/2} \cong r^{\zeta} \tag{4}$$

In the region of validity of Eq. (3), and for rapid crack propagation, it has been postulated that a somehow universal value of the roughness exponent $\zeta = 0.8$ exists, regardless of the material, microstructure, or load conditions [13–16]. One of the objectives of this work is precisely to provide more evidence that could lead either to accept or reject this hypothesis.

There are several methods for the evaluation of the self-affine exponent of height profiles, being the variable bandwidth method relatively simple, precise and accurate [9]. In this method, a profile of length L is divided into windows or 'bands' of width r indexed by the position of the first point of the band, $i = 1$. The standard deviation of the heights, $\sigma(i)$, is computed on each band and then averaged over all the possible bands varying the origin at fixed r following Eq. (5) [9]

$$W(r) = \left(1/N_{\mathrm{d}}\right) \sum_{i=1}^{N\mathrm{d}} \sigma(i) \tag{5}$$

where N_{d} is the number of points. The roughness exponent ζ is obtained from the log–log plot of $W(r)$ vs r according to Eq. (6) [9]

$$W(r) \cong r^{\zeta} \tag{6}$$

The average roughness exponent is then calculated performing a linear regression over the straight interval of all the log–log plots. The length of the extracted profiles could be as largest as the number of points (pixels) that the instrument can detect. In our case, the AFM employed provides a 512 pixels per profile length.

Concerning the polymeric material surfaces, there is still only a few experimental work reported in the literature about their fractal and self-affine behavior. Tzoganakis, using digital image processing techniques [6], has obtained the fractal dimension of a linear low density polyethylene extrudate surface as a quantitative

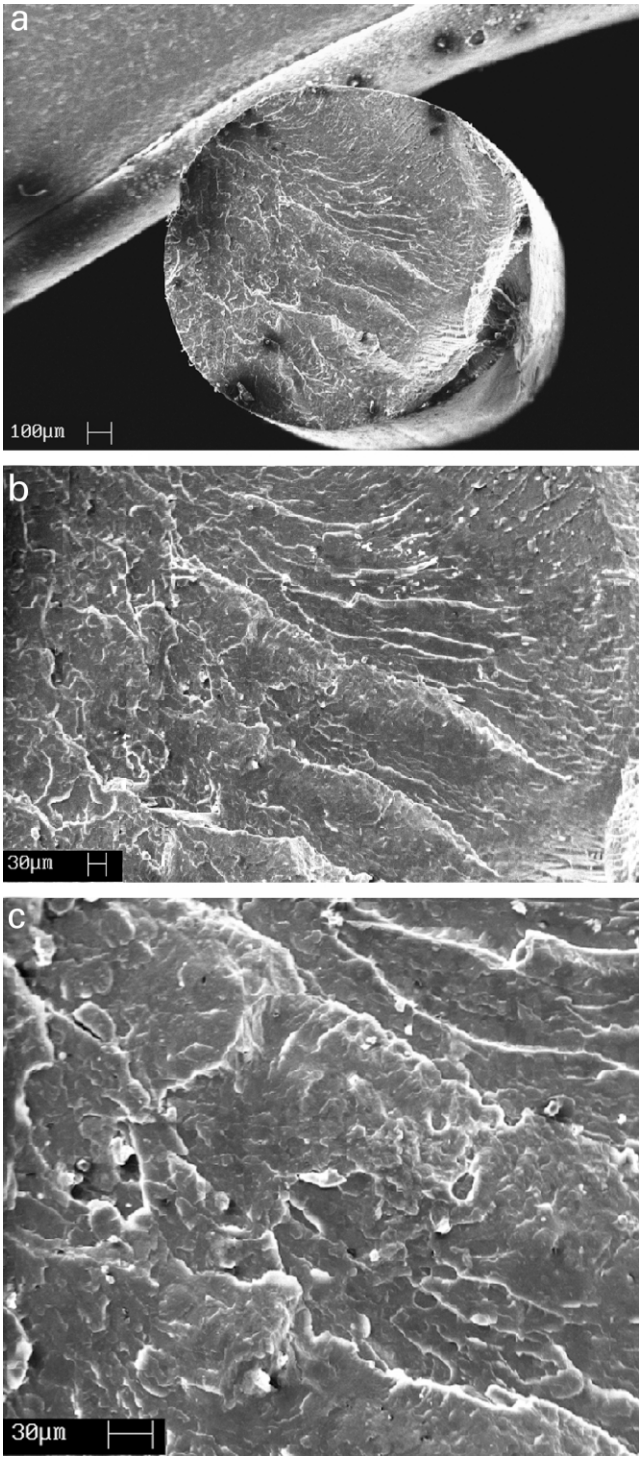

Fig. 5. SEM micrographs of PP fracture surfaces at several magnifications. (a) 100 ×, (b) 250 ×, (c) 500 ×.

measure of its roughness. An attempt has been made to correlate this dimension with the shear stress in capillary extrusion. Using optical microscopy, Chen [2] analyzed a relationship between the fracture toughness of polystyrene (PS) and the fractal dimension of the fracture surface. More recently Smith [17], Guerrero [18] and González [19] have used the AFM

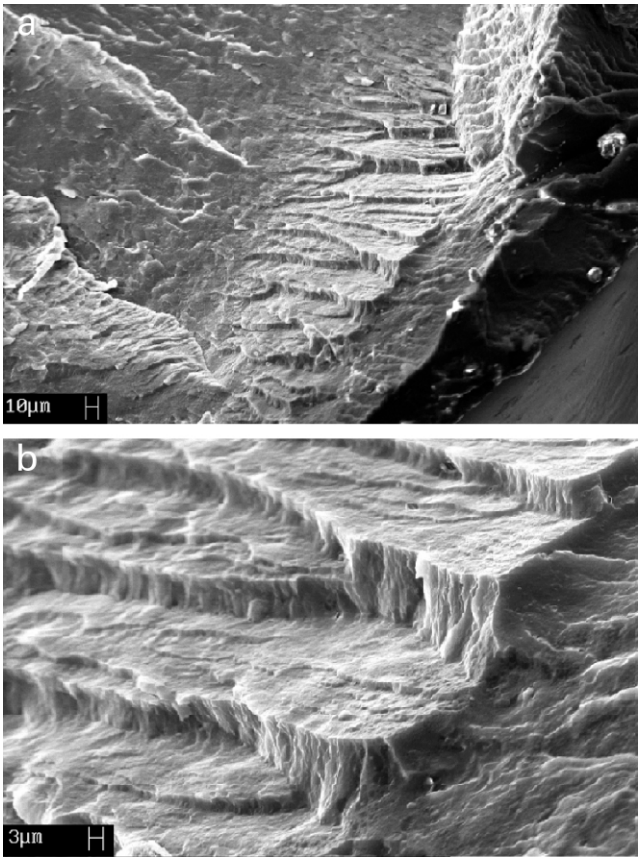

Fig. 6. Propagation of the crack across different planes (uncontrolled fracture). (a) 500 ×, (b) 2000 ×.

for the roughness measurement of the surface of different plastics. Polyethylene films produced by blown film extrusion [17] were examined and a correlation between the mean surface roughness and haze was sought. The roughness exponent of film surfaces of polypropylene (PP), polystyrene, and polyethylene terephtalate, was measured in order to find the appropriate operating conditions of the AFM in contact mode [18]. An attempt was also made to correlate the crystallization rate with the roughness of the polypropylene films [19]. Schmittbuhl [20] reports the static and dynamic evolution of cracks in a block of polymethyl-methacrylate under different loads, determining the roughness exponent.

In this work, we focused our attention on the analysis of the self-affine behavior of fracture surfaces of semi-crystalline polypropylene and amorphous polystyrene, determining their roughness exponent, ζ. The fracture surfaces were produced at conditions—high speed crack propagation—that, according to the literature [13–16], have produced a value of $\zeta \approx 0.8$. Our purpose is to provide more elements confirming that this assumption applies to polymeric materials. The roughness exponent of the fracture surfaces was calculated using the height profiles obtained with the aid of an atomic force microscope, and processed applying the variable bandwidth method. This method offers a very

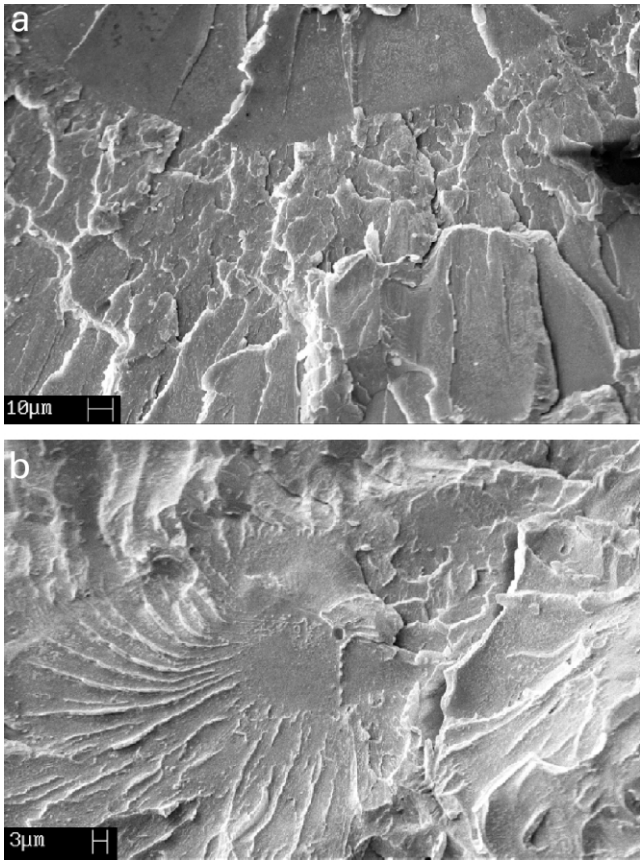

Fig. 7. SEM micrographs of PS fracture surfaces showing (a) the mirror and (b) the hackle zones.

good accuracy and precision when the standard deviation criterion is applied [9].

2. Experimental

The materials used were a semi-crystalline PP and an amorphous PS. The physical properties of both polymers are shown in Table 1 [21]. Samples of these materials were obtained by capillary extrusion at 180 °C for PS and 190 °C for PP. Filaments (about 1 mm diameter and 20 mm length) were randomly selected and cooled to room temperature. After that, specimens were immersed in liquid nitrogen for about 15 min. Fracture surfaces were generated by bending without control of the applied load. That produces a high enough crack propagation speed without preferential direction. For scanning electron microscopy analysis

Table 1
Physical properties of analyzed polymers [21]

Materials	Mn (g/mol)	Polydispersity	T_g (°C)	T_m (°C)	Crystallinity (%)
PP	60,359	5.1	–	165.4	47
PS	76,775	3.1	86	–	–

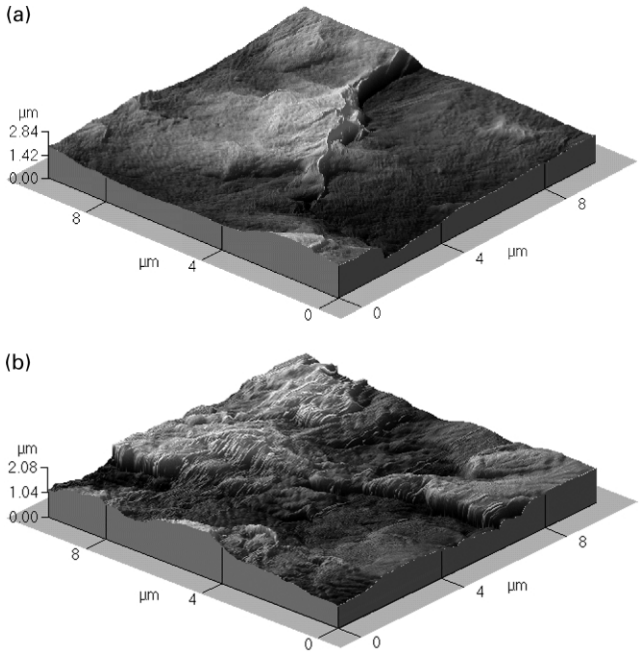

Fig. 8. 3D images of the PP fracture surface at different locations.

(SEM LEO Stereoscan 440), some samples of both fractured polymers were gold sputtered.

The topographical data were obtained using an AFM in contact mode without vacuum (Park Scientific Instruments), varying the scan size from 2.3 to 10 µm. The cantilever tip had a force constant of 0.05 ± 0.02 N/m [21]. For each image, a determined number of profiles uniformly spaced along the scanning direction were selected. See Fig. 1. For each profile, the roughness exponent was then calculated using the variable bandwidth method [9,22].

The accuracy on the estimation of the roughness exponent is strongly dependent on the number of profiles, N_p, involved in the analysis. Therefore, preliminary tests were developed varying the number of profiles considered on the calculus of the average roughness exponent. A plot of this parameter vs N_p was then constructed.

In accordance with the spacing between the tip and the surface sample, there are two modes to operate the AFM: the contact mode (C-AFM) and the non-contact mode (NC-AFM). In the former, the tip rides on the sample in close contact with the surface. The force on the tip is repulsive with a mean value of 10^{-9}–10^{-6} N. In NC-AFM the tip is scanned over the surface with a spacing of 50–150 Å. The force on the tip is attractive with a value close to 10^{-12} N. Because these forces are smaller than those measured with C-AFM, the cantilever must be stiffer. These facts, small forces and great stiffness, are advantageous to the study of soft and elastic materials. However, the signal is difficult to measure. At lower frequencies, slower the scanning, but better the signal. However, it could be possible that dust adheres to the tip, polluting the signal and the measurement. Furthermore, the humidity of the air leads to the formation of a thin layer of liquid over the

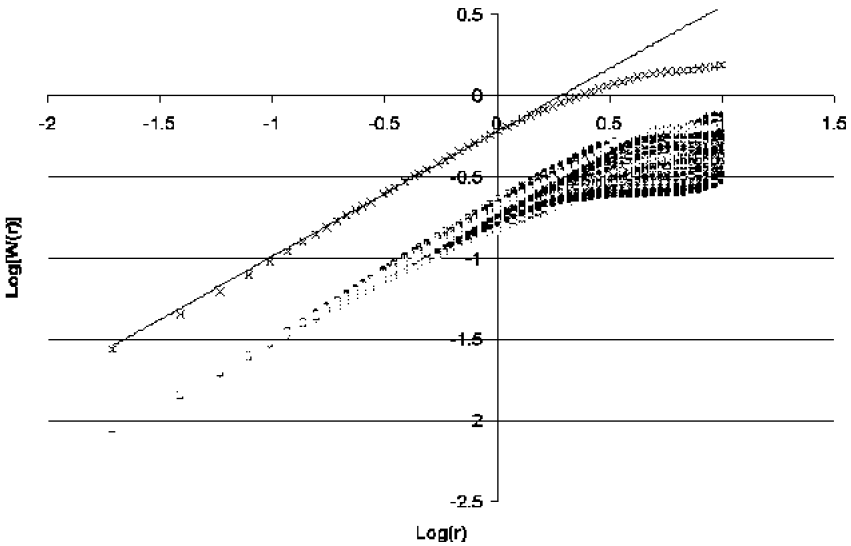

Fig. 9. Results of the self-affine analysis applied to the image in Fig. 8b. The roughness exponent was $\zeta = 0.771 \pm 0.05$.

surface of the sample and capillary forms when the tip dips into the film. Nowadays, when polymeric materials are involved, the trend is to use the NC-AFM technique. In spite of this, we consider that, providing the appropriate operating conditions, C-AFM could be used without surface damage of the samples. Keeping this in mind, and prior to image analysis, the AFM operating conditions in contact mode, i.e. scanning frequency and contact force, were determined. The most important qualitative restriction was to obtain sharp and clear 3D images of the polymer surfaces without causing any harm to the specimens by the microscope tip. Therefore, thin film samples of PP and PS were made placing polymer pellets between two glass-cover plates and pressed for 1 min on a hot plate press at a pre-fixed temperature. The obtained films were then cooled at room temperature for five minutes. Then, they were re-heated on a hot plate for about 30 s. The samples were finally cooled to room temperature. AFM images, at different forces and frequencies, were obtained from these PP and PS film samples.

3. Results and discussion

Computer programs developed at our facilities [9] were used to generate a set of 250 synthetic profiles with 512 points length each one, with a prescribed roughness exponent varying from 0.1 to 0.9. The convergence of the Weierstrass–Mandelbrot function was the method employed for the profiles generation [23]. The value of ζ was calculated for each synthetic profile and then averaged varying the number of profiles involved in the calculus. It could be seen from Fig. 2, that the use of less than 50 profiles on the average estimation could leads to wrong values of ζ. On the light of these tests it was concluded that, in order to ensure a good reproducibility on the average ζ estimation, at least 100 profiles from each AFM image to be analyzed are necessary, see Fig. 2.

For selecting the AFM operating conditions, the starting point was the settings commonly used for the analysis of rigid surfaces, i.e. contact forces around 10^{-6} N and scanning frequencies in the order of 2.0–6.0 Hz [24,25]. For all the analyzed PP and PS film samples the best, clear and sharp, 3D images were obtained with a contact force of $8–15 \times 10^{-10}$ N and a scanning frequency range of 1–1.5 Hz. Then, all the following images in this work were obtained keeping these values as operating conditions. Selected AFM images are shown on Figs. 3 and 4.

In Fig. 3, the spherulitic crystallization of the PP film surface at two scan sizes can be observed, the radial growth of lamellas and the boundaries between neighboring spherulites are clear. Spherulitic size was measured obtaining a diameter on the range of 3–8 μm. Fig. 4 presents, at different film zones and several scan sizes, images of an amorphous polymer surface. These PS images show, in all the analyzed zones, an absence of crystalline order. This morphology mainly results from the processing and cooling conditions. In all cases, figures show sharp and clear images with no evidence of any damage on the film surfaces.

Fracture surfaces were analyzed using both SEM and AFM. Qualitative SEM observations of PP fracture surfaces at several magnifications are shown in Fig. 5. It could be seen curved lines that seem to depart from a point where the cracks started. These lines, named Chevron marks, are particularly useful in assessing the direction of crack propagation and, by inference, the location of the crack origin. At the end of the Chevron marks the morphology changes, making evident the impossibility of the crack to propagate across one plane only, see Fig. 6—uncontrolled fracture. For PS amorphous samples the Chevron marks are also observed, but the sequence of crack propagation,

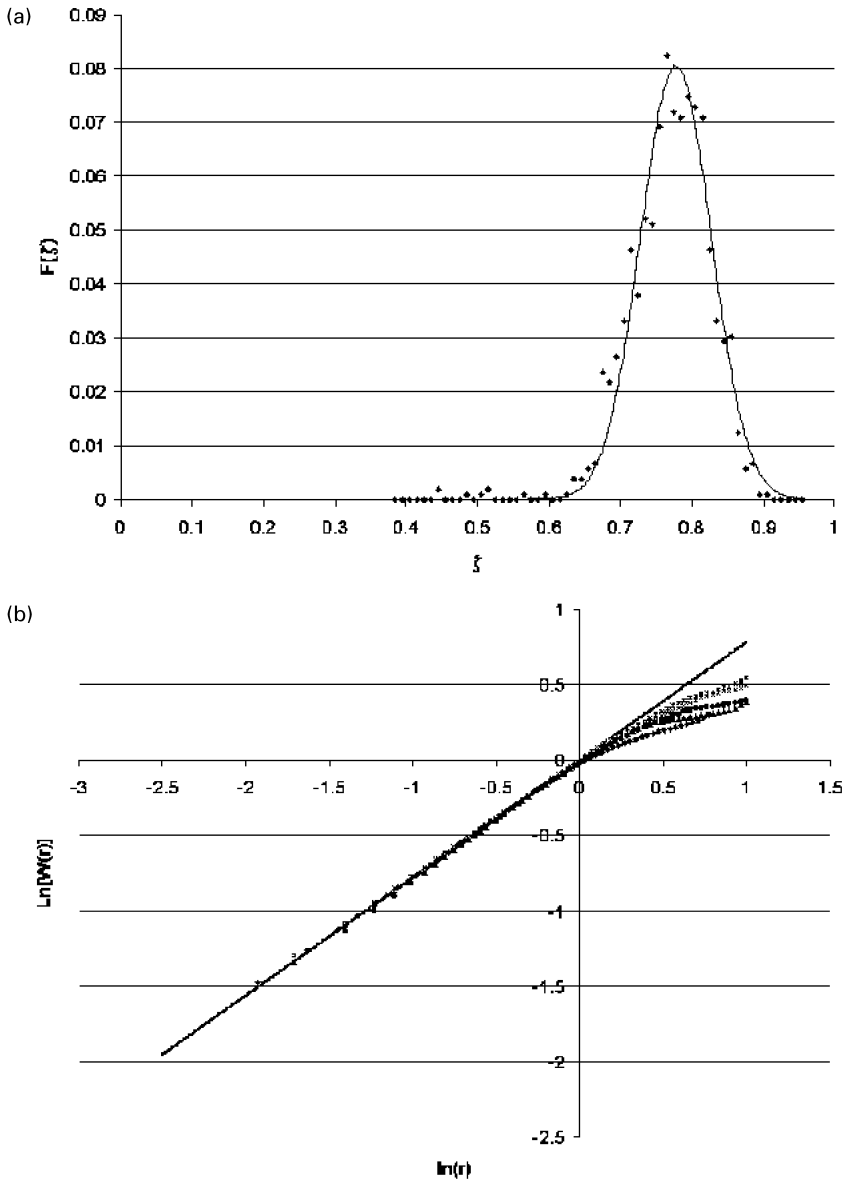

Fig. 10. (a) Normal distribution curve corresponding to the roughness exponent calculated with at least 930 profiles from different images. (b) Average roughness exponent calculated considering all the extracted profiles from all the images; $\zeta = 0.77 \pm 0.09$.

surrounding the fracture initiating crack, involves transitions from an apparent smooth region—the mirror zone—to a slightly rougher region—the mist zone—to a microscopically rough region—the hackle zone. See Fig. 7. This behavior is characteristic on fracture surfaces in amorphous polymers and it is also reported in other amorphous brittle materials such as inorganic and organic glasses [26]. The radiating patterns of lines on the PS fracture surface, Fig. 7b, reveals the crack origin.

In all the analyzed SEM images, the fracture surfaces present similar morphologies at different magnifications. This could be considered as qualitative evidence of self-affine behavior.

Fig. 8 shows typical 3D AFM images of the PP fracture surface at several locations; the irregularity of the surfaces is perfectly observed. Each image consists of a series of height profiles which resolution (distance between two consecutive points) is function of the scan size, provided the image is always 512 pixels long. The shortest measured profiles were 3.5 μm long, giving a resolution of about 7 nm.

The self-affine analysis applied to one of the images of the *i*-PP fracture surfaces, Fig. 8b, is presented on Fig. 9. Each set of data on the bottom of the figure corresponds to the measured values from one profile and the average roughness exponent, calculated via a linear regression over the straight interval of all the log–log plots (232 profiles), was in this case $\zeta = 0.771 \pm 0.05$. The excellent fitting to a straight line, over more than three decades, in all the analyzed images is an indicative of the self-affine behavior of the fractured surfaces. However, considering the strong statistical nature of the self-affine objects, it was decided to compute normalized distributions with the self-affine

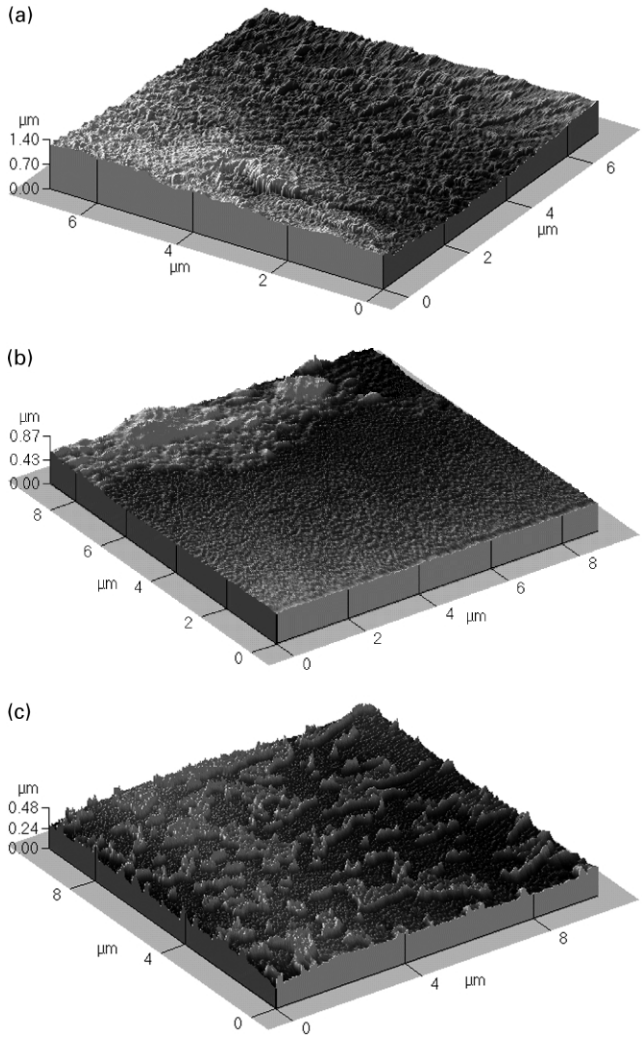

Fig. 11. 3D images of the PS fracture surfaces: (a) morphology very similar to those encountered on PP samples; (b) transition from the mirror zone to the hackle zone; (c) patch morphology.

exponent of all the extracted profiles from all the fractured surfaces. Fig. 10a shows the normal distribution curve corresponding to self-affine exponents calculated from different images. It could be seen a unimodal curve that could be very well fitted to a normal Gaussian distribution. Fig. 10b presents the average self-affine exponent calculated considering all the extracted profiles from all the images. The slope of the straight line was $\zeta_{av} = 0.77 \pm 0.09$.

Impurities and other defects that could be attributed to sample handling could modify, for the same specimen, both the frequency distribution of the self-affine exponent and its average value. However, the size of the analyzed population minimize, statistically speaking, the effect of the observed impurities (AFM images show just a little evidence of impurities). In fact, the frequency distributions obtained experimentally adjust very well with a Gaussian distribution, providing this a high degree of confidence in our results.

Some 3D images of PS fractured samples are shown on Fig. 11. The irregular pattern on Fig. 11a is similar to those encountered on PP samples, while Fig. 11c shows the so called 'patch' morphology, which results from the removal of isolated patches of craze material from each half of the fracture surface. The 'hackle' region is mainly formed by a patch morphology. For PS samples, the same self-affine analysis applied to *i*-PP samples was done. Fig. 12 shows the results obtained for the images presented on Fig. 11. From these plots, it could be seen a restricted zone, at lower '*r*' values, where a straight line can be drawn; its slope has a value of around 0.7. The restricted zone is placed between $r = 10^{-2}$ and 10^{-1} μm, only one decade length. After that it seems that the system presents no more self-affinity. This behavior was corroborated with the analysis of at least nine PS images, covering more than 2000 different profiles. The average roughness exponent (slope of the straight line) was found to be $\zeta_{av} = 0.707 \pm 0.07$, see Fig. 13, expanded over just one decade length.

Intuitively, it can be expected that two objects of the same polymer, molded under the same conditions can differ in fracture plane characteristics, leading this to a different value of roughness exponents. In fact, the morphology of fracture surfaces is strongly dependent on the material, its fracture mechanism and the scale of observation, but the statistical characterization of the topology of the fracture surfaces leads to a scale invariance; these surfaces exhibit statistically self-affine scaling properties. In our case, we conjecture that the surface plane characteristics do not determine the roughness exponent; two different self-affine objects could have the same scaling properties and then we could magnify them following the same self-affine exponent, but probably the coefficient of the scaling transformation (λ in Eq. (3)) will be different.

It is reasonable to assume that material properties should affect both the morphology and the scaling of the fracture surface. However, the role of microstructure and its relations with the self-affinity parameters are not well understood. It seems that the roughness exponent is not directly related to the microstructure, instead attempts have been made to relate the self-affine correlation length with microstructure features such as the large heterogenities presented in the microstructure, i.e. the grain size on aluminum alloys [27], the size of the opacifying particles on opal glass [28], or with the collective behavior of the point defects introduced by ionic exchange on a soda-lime silica glass [29]. At this time, most of our efforts are directed on this field.

4. Conclusions

It was necessary to extract at least 100 profiles from each AFM image to ensure a good reproducibility on the average estimation of the roughness exponent, ζ_{av}.

Using *PP* and *PS* thin film samples, the appropriate AFM operating conditions in contact mode were found. The best

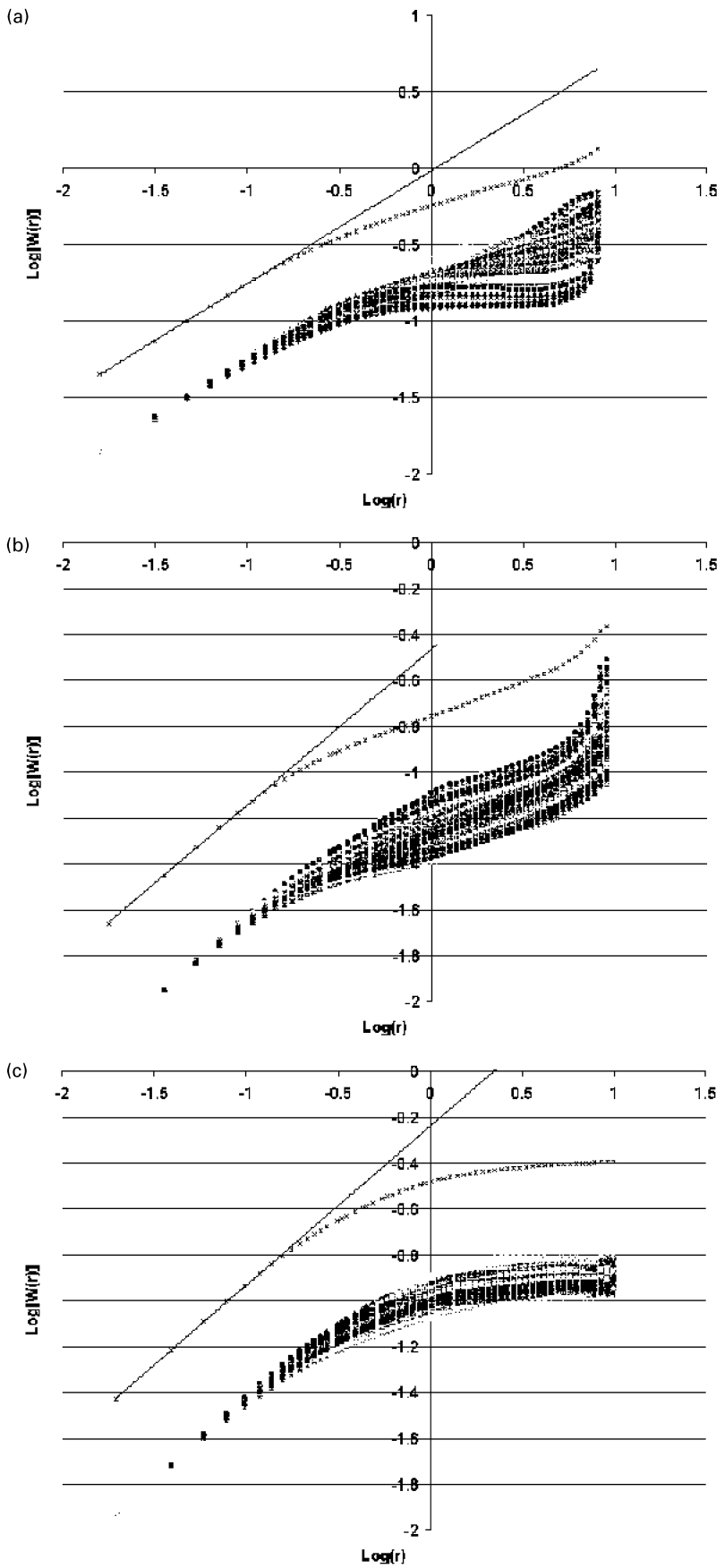

Fig. 12. Self affine analysis of PS samples presented in Fig. 11 (a) $\zeta = 0.738 \pm 0.01$, (b) $\zeta = 0.679 \pm 0.02$ and (c) $\zeta = 0.693 \pm 0.01$. In all cases, the number of profiles considered for the estimation of ζ was 250.

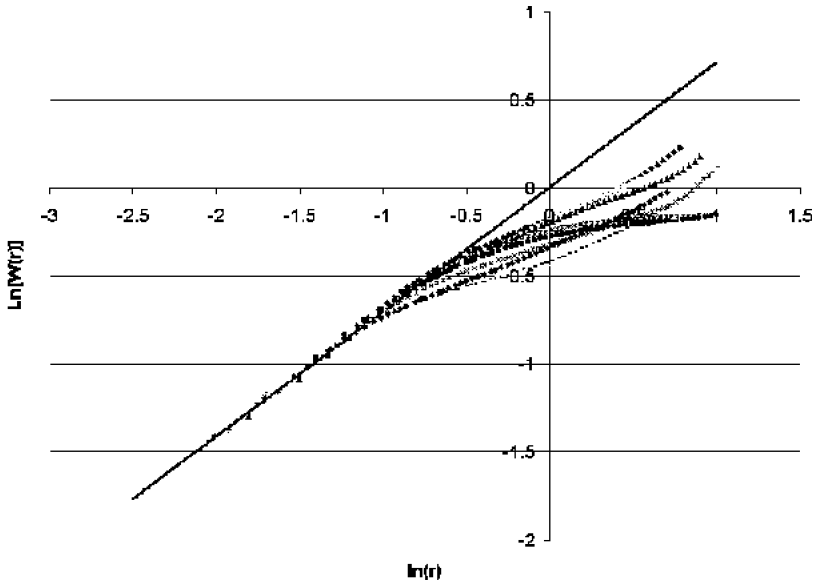

Fig. 13. Average roughness exponent for PS samples, $\zeta_{av} = 0.707 \pm 0.07$.

clear and sharp images were obtained with a contact force range of 0.8–1.5 nN and a scanning frequency range of 1–1.5 Hz.

The fracture surface of semi-crystalline polypropylene exhibits a self-affine behavior with an average roughness exponent of $\zeta_{av} = 0.77 \pm 0.09$, expanded over at least three decades.

The fracture surface of amorphous polystyrene exhibits a self-affine behavior over a very restricted zone, only one decade length. The estimated average roughness exponent was $\zeta_{av} = 0.707 \pm 0.07$.

The roughness exponents found, about 0.77 for polypropylene and 0.71 for polystyrene, are very close to values reported in literature, which have claimed a universal value of 0.8. These results could be then considered as favorable evidence leading to accept the proposed assumption.

Acknowledgements

Financial assistance from the National Science and Technology Council (CONACYT) from México, and the Science and Technology Research Program (PAICYT) from the UANL is greatly appreciated (grants 28188-U and CA-224, respectively).

References

[1] Garbassi F, Morra M, Occhiello E. Polymer surfaces. From physics to technology. Chichester: Wiley; 1998.
[2] Chen CT, Runt J. Polym Commun 1989;30(11):334–5.
[3] Wu Li X, Tian J, Kang Y, Wang Z. Scripta Metall Mater 1995;33(5):803–9.
[4] Mandelbrot BB, Passoja DE, Paullay AJ. Nature 1984;308:721–2.
[5] Pande CS, Richards LR, Lovat N, Dempey BD, Schwoeble AJ. Acta Metall 1987;35(7):1633–7.
[6] Tzoganakis C, Price BC, Hatzikiriakos SG. J Rheol 1993;37(2):355–66.
[7] Reyes E, Guerrero C, González V, Hinojosa M. In: Robertson IM, Lassila DH, Devincre B, Phillips R, editors. Multiscale phenomena in materials—experiments and modeling. Material Research Society Symposium Proceedings, vol. 578. Pennsylvania: Materials Research Society; 2000. p. 357–61.
[8] Hinojosa M, Aldaco J, Ortiz U, González V. Aluminum Trans 2000;3(1):53–7.
[9] González V, Chacón O, Hinojosa M, Guerrero C. Fractals 2002;10(3):373–86.
[10] Magonov SN, Reneker DH. Annu Rev Mater Sci 1997;27:175–222.
[11] Strausser YE, Heaton MG. American Laboratories; 1994.
[12] Parisi A, Caldarelli G, Pietronero L. Condens Matter 2000;4374.
[13] Meisel LV, Scanlon RD, Johnsons MA, Lanzerotti VD. In: Robertson IM, Lassila DH, Devincre B, Phillips R, editors. Multiscale phenomena in materials—experiments and modeling. Material Research Society Symposium Proceedings, vol. 578. Pennsylvania: Materials Research Society; 2000. p. 363–7.
[14] Deng J, He YF, Ye F, Long QY, Lung CW. J Phys D: Appl Phys 1999;32:L45–8.
[15] Hinojosa M, Bouchaud E, Nghiem B. In: Beltz GE, Blumberg RL, Kim KS, Marder MP, editors. Fracture and ductile vs. brittle behavior—theory, modelling and experiment. Material Research Society Symposium Proceedings, vol. 539. Pennsylvania: Materials Research Society; 1999. p. 203–8.
[16] Aldaco J, Garza FJ, Hinojosa M. In: Robertson IM, Lassila DH, Devincre B, Phillips R, editors. Multiscale phenomena in materials—experiments and modeling. Material Research Society Symposium Proceedings, vol. 578. Pennsylvania: Materials Research Society; 2000. p. 351–6.
[17] Smith PF, Chung I, Liu G, Dimitrievich D, Rasburn J, Vancso GJ. Polym Engng Sci 1996;36(16):2129–34.
[18] Reyes E, Guerrero C. Annual technical Conference Proceedings, Society of Plastics Engineers; 2000. p. 3631–4.
[19] González V, Hinojosa M, Guerrero C, Reyes E. Annual technical Conference Proceedings, Society of Plastics Engineers; 2000. p. 3594–8.

[20] Schmittbuhl J, Maloy KJ. Phys Rev Lett 1997;78(20):3888–91.
[21] Reyes E. MSc Thesis. Universidad Autónoma de Nuevo León, Monterrey, México; 1999.
[22] Schmittbuhl J, Vilotte JP, Roux S. Phys Rev E 1995;51(1):131–47.
[23] Feder J. Fractals. New York: Plenum Press; 1988.
[24] Sarid D. Scanning force microscopy. New York: Oxford University Press; 1994.
[25] Howland R, Benatar L. A practical guide to scanning probe microscopy. California: Park Scientific Instruments; 1997.
[26] West JK, Mecholsky JJ, Hench LL. J Non-Cryst Solids 1999;260: 99–108.
[27] Hinojosa M, Aldaco J. J Mater Res 2002;17(6).
[28] Reyes E, Guerrero C, Hinojosa M. In: Novak MM, editor. Emergent nature. Patterns, growth and scaling in the sciences. New Jersey, USA: World Scientific; 2001. p. 385–91.
[29] Garza F, Hinojosa M, Chávez L. In: Novak MM, editor. Emergent nature. Patterns, growth and scaling in the sciences. New Jersey, USA: World Scientific; 2001. p. 393–401.